Validation of an anti-sphingosine-1-phosphate antibody as a potential therapeutic in reducing growth, invasion, and angiogenesis in multiple tumor lineages

Barbara Visentin,[1,5] John A. Vekich,[1,5] Bradley J. Sibbald,[1] Amy L. Cavalli,[2] Kelli M. Moreno,[2] Rosalia G. Matteo,[2] William A. Garland,[2] Yiling Lu,[3,5] Shuangxing Yu,[3,5] Hassan S. Hall,[3] Vikas Kundra,[4] Gordon B. Mills,[3] and Roger A. Sabbadini[1,2,*]

[1] Department of Biology, San Diego State University, San Diego, California 92182
[2] Lpath, Inc., San Diego, California 92121
[3] Departments of Molecular Therapeutics and Radiation Oncology, M.D. Anderson Cancer Center, Houston, Texas 77054
[4] Departments of Radiology and Experimental Diagnostic Imaging, University of Texas M.D. Anderson Cancer Center, Houston, Texas 77054
[5] These authors contributed equally to this work.
*Correspondence: rsabba@sunstroke.sdsu.edu

Summary

S1P has been proposed to contribute to cancer progression by regulating tumor proliferation, invasion, and angiogenesis. We developed a biospecific monoclonal antibody to S1P to investigate its role in tumorigenesis. The anti-S1P mAb substantially reduced tumor progression and in some cases eliminated measurable tumors in murine xenograft and allograft models. Tumor growth inhibition was attributed to antiangiogenic and antitumorigenic effects of the antibody. The anti-S1P mAb blocked EC migration and resulting capillary formation, inhibited blood vessel formation induced by VEGF and bFGF, and arrested tumor-associated angiogenesis. The anti-S1P mAb also neutralized S1P-induced proliferation, release of proangiogenic cytokines, and the ability of S1P to protect tumor cells from apoptosis in several tumor cell lines, validating S1P as a target for therapy.

Introduction

The identification of signaling components that promote tumor growth represents an important step toward discovering new therapies to reduce the morbidity and mortality of cancer. In this regard, the bioactive lysolipid signaling molecule sphingosine-1-phosphate (S1P) is a little-explored target for antitumor treatment. Evidence suggests that S1P may play a major regulatory role in tumor biology by having direct effects both on tumor-associated angiogenesis and on the tumor cells themselves (Ogretmen and Hannun, 2004).

S1P is a mediator of tumor cell proliferation and protects tumor cells from apoptosis through the activation of survival pathways (Maceyka et al., 2002; Spiegel and Milstien, 2003; Radeff-Huang et al., 2004). The balance between S1P and ceramide/sphingosine (CER/SPH) levels, the upstream precursors of S1P, is believed to provide a rheostat mechanism that determines whether a cell proliferates or undergoes apoptosis (Kwon et al., 2001; Maceyka et al., 2002). The key regulatory enzyme of the rheostat mechanism is sphingosine kinase (SPHK), whose role is to convert the death-promoting sphingolipids (CER/SPH) into the growth-promoting S1P (Bektas et al., 2005). Indeed, SPHK1 transfectants produced tumors when injected into mice (Xia et al., 2000). Furthermore, cells overexpressing SPHK escape contact inhibition, a property commonly exhibited by transformed cells. The reported loss of contact inhibition is consistent with reports suggesting that S1P production correlates with the metastatic potential of selected human cancer cell lines (Takuwa, 2002; Yamaguchi et al., 2003). Additionally, high levels of SPHK1 expression in certain tumor tissues correlate with lower patient survival, thus suggesting a connection between SPHK1 and the aggressiveness of these tumors (Van Brocklyn et al., 2005).

S1P contributes to angiogenesis (Allende and Proia, 2002; Argraves et al., 2004) by stimulating DNA synthesis, chemotactic motility, and capillary tube formation of endothelial cells (ECs)

SIGNIFICANCE

The data suggest that S1P is required for the neovascularizing activity of VEGF and bFGF as well as angiogenesis induced by multiple cytokines. Thus, neutralizing S1P with anti-S1P monoclonal antibodies has the potential to block neovascularization in multiple tumor lineages and is less likely to be bypassed by production of multiple factors than are other approaches to targeting tumor vessels. Further, the data suggest that S1P is required for proliferation and invasion of multiple tumor lineages. Thus, the anti-S1P mAb warrants clinical evaluation to determine its efficacy in reducing cancer progression by neutralizing the proliferative, invasive, and angiogenic effects of S1P. Thus, the anti-S1P mAb may represent a noncancer type-specific therapy for use in humans.

and bone marrow-derived EC precursors, processes that contribute to early blood vessel formation (Lee et al., 1999). The capillary tube formation induced by S1P is comparable to that of the well-known proangiogenic mediators basic fibroblastic growth factor (bFGF) and vascular endothelial growth factor (VEGF) (Lee et al., 1999). Furthermore, S1P elicits synergistic effects with these growth factors to promote development of vascular networks in vivo (Wang et al., 1999). Recently, crosstalk between S1P and other proangiogenic growth factors such as VEGF, EGF, PDGF, bFGF, and IL-8 has been reported (Schwartz et al., 2001; Spiegel and Milstien, 2003). Importantly, bevacizumab (Avastin), a monoclonal antibody that selectively absorbs VEGF from the extracellular fluid (Ferrara, 2004), demonstrated efficacy in limiting the progression of three major types of human cancer. The success of Avastin has stimulated an exploration for similar and more efficacious targets to block tumor-associated angiogenesis. Since S1P is required for the optimal activity of multiple proangiogenic factors, S1P is a promising target for novel therapeutic approaches.

These findings indicate that lowering the interstitial concentration of S1P in tumors could provide a less favorable growth environment for cancer cells by decreasing angiogenesis, while decreasing proliferation and metastatic potential and increasing sensitivity to apoptosis. For this reason, we have produced a monoclonal antibody against S1P (anti-S1P mAb) that is specific to S1P and can bind and neutralize extracellular S1P at its physiologically relevant concentrations. In addition to providing a sensitive probe of the in vivo function of S1P, we hypothesize that this antibody could prove useful as a therapeutic molecular sponge to selectively absorb S1P, thus lowering effective extracellular concentrations of this tumor growth factor.

In this study, we demonstrate that neutralization of S1P results in the reduction of tumor growth through multiple mechanisms including reduced tumor proliferation, cell survival, and metastatic potential concurrently with reduced vessel formation and function. The efficacy of the molecular absorption of S1P in these models suggests that treatment with a humanized version of the murine anti-S1P antibody may provide an innovative and useful approach to cancer therapeutics.

Results

Characteristics of the anti-S1P mAb

Competitive ELISA was used to determine the specificity and sensitivity of the anti-S1P mAb. Figure 1A shows that the anti-S1P mAb was capable of recognizing S1P over the range of S1P concentrations used in the cell-based experiments described below. The anti-S1P mAb was unable to recognize the structurally related bioactive lysolipid lysophosphatidic acid (LPA) or the bioactive precursor to S1P, SPH. Other lysolipids and phospholipids including CER, ceramide-1-phosphate (C1P), and phosphatidyl ethanolamine (PE) were tested without observing appreciable antibody crossreactivity with the exception of the fully saturated form of S1P,DH-S1P, and modest crossreactivity with sphingosylphosphoryl choline (SPC). Neutralizing SPC as well as S1P with the antibody could be advantageous because SPC itself is tumorigenic (Beil et al., 2003). However, extracellular levels of SPC are low, likely due to the presence of autotoxin which has recently been shown to convert SPC to S1P (Clair et al., 2003).

A study utilizing BIAcore demonstrated that the anti-S1P mAb has an affinity for S1P of 99.7 ± 14.4 pM (SD; n = 3). This affinity is over 100-fold higher than the reported affinity of S1P receptors for S1P and much higher than the nonspecific binding sites on serum proteins (Richieri et al., 1993).

To determine the dosing for subsequent in vivo experiments, the in vivo $t_{1/2}$ of the anti-S1P mAb was determined. A competitive ELISA was used to determine the pharmacokinetics of the anti-S1P mAb in blood. Figure 1B shows the time course of the anti-S1P mAb elimination with the dosing of 25 mg/kg. Using a standard two compartment model calculation in WinNonlin, a $t_{1/2}$ (elimination) of 20–26 hr was determined. This $t_{1/2}$ is consistent with the pharmacokinetic profiles of other therapeutic antibodies (Ignoffo, 2004). A simulation of dosing of 25 mg/kg anti-S1P mAb every 2 days demonstrated the concentrations of antibody in the mouse that did not significantly accumulate over time (Figure S1 in the Supplemental Data available with this article online). Intraperitoneal injection of a bolus dose of the anti-S1P mAb revealed that over 95% of the antibody appeared in the bloodstream after 20 min, suggesting that mice could effectively be dosed either intraperitoneally (i.p.) or intravenously (i.v.). We have calculated that the molar ratio of anti-S1P mAb to plasma S1P is ~3:1 at the 25 mg/kg dose injected into a 20 g mouse and assuming a plasma volume of 1.4 ml with a S1P concentration (total) of 2.45 μM.

We conducted a 7 day toxicology study to determine how the antibody was tolerated. Mice were administered (by tail vein injection) 1, 3, 10, 30, or 50 mg/kg of the anti-S1P mAb or vehicle for 7 consecutive days. Figure 1C demonstrates a few selected parameters for the 50 mg/kg and saline dosing. All biochemical and CBC panel analyses were within normal ranges. Histopathological examination revealed no lesions or other pathological changes in the liver, kidney, heart, lungs, skeletal muscle, or spleen of mice in any dosing group. Mice in all treatment groups consumed food and water and socialized similarly to control animals. In one of the xenograft studies described below, mice were administered i.p. 25 mg/kg of the anti-S1P mAb every other day for up to 6 weeks. Even though this was not a bona fide toxicology study, mice in this study exhibited no prominent abnormalities of the major organs upon sacrifice.

Anti-S1P antibodies slow tumor progression in multiple murine models

The ability of the anti-S1P mAb to inhibit cancer progression was tested in three orthotopic models using the breast carcinoma cells MDA MB-231 and MDA MB-468, and the ovarian cancer cell line SKOV3. The anti-S1P mAb was also tested in a subcutaneous xenograft model using lung adenocarcinoma A549 cells.

Figures 2A and 2B show the effects of the systemic anti-S1P mAb treatment on MDA MB-231 multidrug-resistant breast carcinomas orthotopically placed in the mouse mammary fat pads (Figure 2A). The ability of the anti-S1P mAb to reduce tumor volumes was most apparent after the tumors reached approximately 400 mm^3, where tumors of the anti-S1P mAb-treated animals nearly stopped growing. At the end of the study, MDA MB-231 tumor volumes and weights were reduced by 62% and 40% (Figure 2A; *$p < 0.001$), respectively. The anti-S1P mAb was as effective as weekly paclitaxel in decreasing tumor volume in these mice (data not shown).

In a similar orthotopic breast cancer study (Figure S2), MDA MB-468 tumor volumes were reduced by 40% with respect to

A

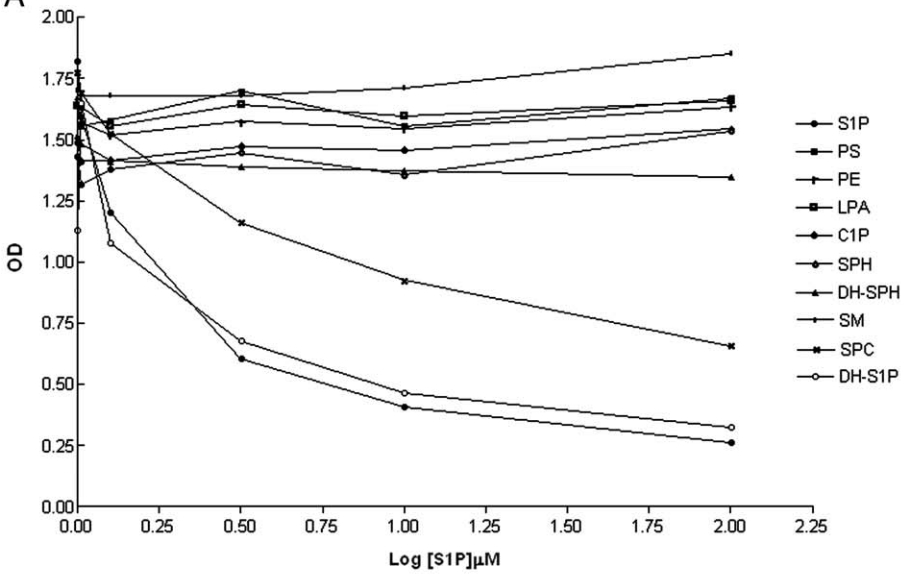

B

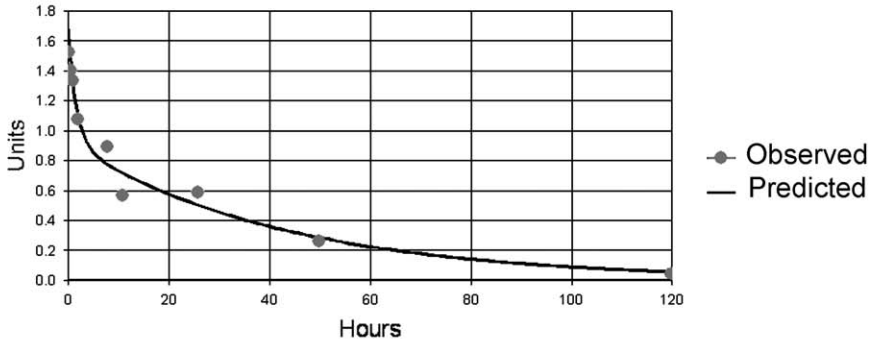

C

Selected Toxicological Results: Mean ± SD.		
Selected Parameters	**Control**	**50mg/kg Anti-S1P mAb**
Weight on day 1 (g)	18.6 ± 0.4	19.1 ± 0.7
Weight on day 7 (g)	19.6 ± 0.6	20.6 ± 0.8
Food Intake (pellets/day)	1.08 ± 0.2	1.11 ± 0.1
WBC (thou/μL)	5.87 ± 2.6	3.43 ± 0.3
RBC (mil/μL)	8.83 ± 0.3	9.34 ± 0.5
Alk Phosphatase (IU/L)	94.5 ± 36.1	58.0 ± 35.4
CK (IU/L)	5154 ± 1765	6906 ± 5023
Albumin (g/dL)	3.3 ± 0.01	3.1 ± 0.3
Total Bilirubin (mg/dL)	≤0.3	≤0.3
BUN (mg/dL)	22.5 ± 2.1	23.7 ± 1.5

Figure 1. Characteristics of the anti-S1P mAb

A: Competitive ELISA demonstrating the ability of the anti-S1P mAb to recognize S1P but not LPA, SPH, or other related lipids.

B: Mice were treated with a bolus dose of 25 mg/kg of the anti-S1P mAb. The elimination $t_{1/2}$ of the antibody, as determined by the concentration of mAb in the serum at designated time points using a competitive ELISA, was calculated to be 22–26 hr.

C: Represented toxicological data from mice (four in each group) dosed i.v. every day with 50 mg/kg anti-S1P mAb. Values are means ± SD and demonstrate the lack of adverse effects elicited by the anti-S1P mAb.

saline controls (*$p < 0.05$). These data confirm the efficacy of the anti-S1P mAb against two human multidrug-resistant orthotopic breast cancer models.

We next evaluated the ability of the anti-S1P mAb to alter the progression of larger and very well-established tumors (Figure 2). In the orthotopic MDA MA-231 model, tumors were allowed to establish until they reached an approximate volume of 700–800 mm^3 (10-fold larger than those used in Figure 2A) before antibody (specific or nonspecific) treatments were commenced. As shown, the anti-S1P mAb-treated animals exhibited significantly reduced tumor volumes. By the 14th day, the final tumor volumes from the anti-S1P mAb-treated mice were reduced by over 58% (*$p < 0.001$) by comparison to tumors from control mice. After 2 weeks, the treatment was ceased in half of the mice receiving the anti-S1P mAb, and the progression of the tumors was evaluated for 12 additional days. After a delay of 3 days, tumors from the mice no longer receiving the anti-S1P mAb once again started to grow compared to tumors from

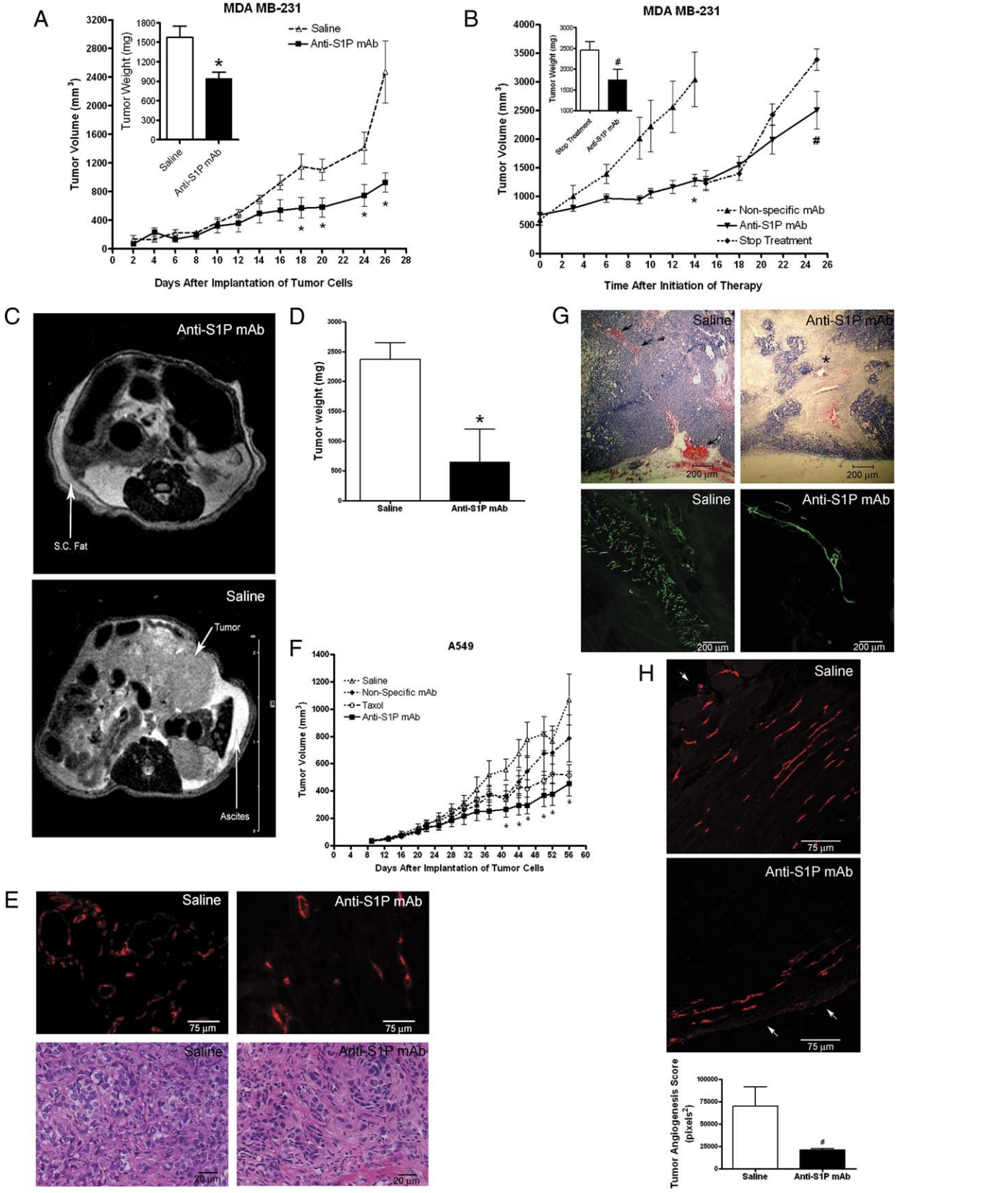

Figure 2. The anti-S1P mAb reduces tumor progression in multiple models

Orthotopically placed MDA MB-231 (**A** and **B**), SKOV3 (**C**–**E**), and s.c. A549 (**F**) tumors were established to volumes of 75–100 mm^3 (**A**, **C**, and **E**) or 700–800 mm^3 (**B**) in nude mice. Treatments consisted of 25 mg/kg of the anti-S1P mAb, 25 mg/kg of nonspecific mAb, saline administrated every 3 days i.p., and 10 mg/kg of Taxol administrated once a week. In all tested xenografts, the anti-S1P mAb reduced significantly final tumor volumes (mm^3) by 62% (**A**), by 58% (**B**), and by 42%

animals maintained on antibody treatment. This lag suggests that the $t_{1/2}$ of 26 hr (see Figure 1B) was likely an underestimate of the physiological half-life of the effective antibody dose.

Figures 2C–2E demonstrates that the anti-S1P mAb was efficacious in inhibiting the progression and, in some cases, eliminating orthotopic SKOV3 tumors in nude mice. MRI analysis revealed that all saline control mice contained large tumors throughout the peritoneal cavity and that these mice had accumulated observable amounts of ascites. Conversely, in two out of the five animals treated with the anti-S1P mAb, no tumors or ascites were detected by MRI analysis or upon postmortem dissection of the peritoneal cavity. Three out of the five animals treated with the anti-S1P mAb had detectable tumors; significantly, these tumors were 68% smaller (750 mg versus 2300 mg) than tumors from the saline-treated animals (*$p < 0.05$). These results compare favorably to a very similar study showing that mouse anti-human VEGF mAb (A.4.6.1) produced a 47% reduction in the size of SKOV3 tumors by MRI (Gossmann et al., 2000). The SKOV3 intraperitoneal model was also assessed for CD31 and H&E staining (Figure 2E). Anti-CD31-labeled sections (upper panel) showed a marked decrease in EC staining of tumor vessels in the anti-S1P mAb-treated mice (representative mouse of five analyzed). Further, H&E staining (lower panel) revealed evidence of increased fibrosis in anti-S1P mAb-treated mice.

Figure 2F shows data using xenografted A549 lung carcinoma cells where the A549 tumor volumes were significantly (*$p < 0.05$) reduced in the antibody-treated animals when compared to animals treated with saline as a control (58% reduction) or animals treated with the nonspecific antibody (42% reduction). The ability of the anti-S1P mAb to retard tumor growth was equivalent to mice treated with Taxol as a positive control. The excised tumors were evaluated for histopathological features in order to determine the full extent of the anti-S1P effects on the viability of remaining tumor cells. H&E-stained sections of the A549 tumors revealed that the tumors from the anti-S1P mAb-treated animals exhibited larger necrotic cores as well as extensive fibrosis (Figure 2G, top panel). Only the tumor peripheries showed appreciable numbers of viable tumor cells. Histological examination indicated that the measurements of gross tumor volumes seen in Figure 2F may have underestimated the actual antitumorigenic effects of the anti-S1P mAb, considering that gross tumor volumes also take into account the volume occupied by dead cells and fibrotic tissue (as also seen in the SKOV3 tumors; Figure 2E). In both control and anti-S1P mAb-treated animals, the vascularization within each tumor was largely confined to the viable regions of the tumor at the periphery rather than in the necrotic core. The extent of tumor-associated angiogenesis was largely mitigated by the anti-S1P mAb treatment, as evidenced by the overall lack of robust microcapillary staining with the isolectin (Figure 2G, bottom panel). In parallel experiments, EC staining with anti-CD31 revealed substantial (3.3-fold) and significant ($^{\#}p < 0.05$) reductions in EC presence in the A549 tumors of anti-S1P mAb-treated animals (Figure 2G), similar to the CD31 staining of the SKOV3 tumors (Figure 2E).

Taken together, these in vivo xenograft models demonstrate that the observed antitumor effects of the anti-S1P mAb were not cancer type specific. Furthermore, the efficacy of the anti-S1P mAb in slowing tumor progression was not dependent on the size of the tumors at the initiation of treatment. Thus, S1P appears to play a major role in tumorigenesis and vascularization in multiple tumor lineages.

The anti-S1P mAb inhibits the release of proangiogenic growth factors in vitro and in vivo

Figure 3A demonstrates that 1 μM S1P induced substantial (2- to 4-fold) increases in IL-6, IL-8, and VEGF release from MDA MB-231 cells in vitro. Figure 3A also demonstrates that treatment of cells with S1P after preincubation with the anti-S1P mAb caused a reduction in the extent of cytokine release to basal levels or less. Secreted VEGF levels were nearly undetectable after antibody treatment, suggesting a potential autocrine stimulatory loop in MDA MB-231. S1P also elicited significant release of IL-8 into the cell-conditioned media from cultured SKOV3 and OVCAR3 cells, and addition of the anti-S1P mAb reduced IL-8 release from all tumor types in a concentration-dependent manner (Figure S3).

Figure 3B demonstrates that serum from MDA MB-231 and SKOV3 xenografted animals displayed substantial levels of the three human cytokines, IL-6, IL-8, and VEGF. Consistent with the in vitro observations of Figure 3A, animals treated with the anti-S1P mAb had significantly reduced (2- to 4-fold) levels of all circulating proangiogenic cytokines tested. Both the in vitro and in vivo data demonstrate that one of the effects of S1P on angiogenesis may be its ability to induce the release of a variety of other proangiogenic compounds.

The anti-S1P mAb blocks the function of proangiogenic growth factors in vivo

Figure 4 compares the proangiogenic activities of S1P, bFGF, or VEGF in vivo when added to the Matrigel plugs. Figure 4A shows that all three growth factors induced substantial evidence of vascularization compared to control animals whose plugs were lacking the growth factors. Notably, S1P was as potent as VEGF and bFGF used at their optimum concentrations in the Matrigel plug assay.

Endogenous S1P has been shown to act synergistically with other growth factors such as bFGF and VEGF in stimulating angiogenesis (Licht et al., 2003). We hypothesized that endogenous S1P from the blood and surrounding tissue may represent an additional proangiogenic factor to supplement plugs containing either VEGF or bFGF. To evaluate these hypotheses, mice implanted with plugs containing VEGF or bFGF received injections of the anti-S1P mAb. Figure 4B shows representative examples of plugs where the neovascularization effects of either

and 58% (**F**). Inset figures represent final tumor weights (mg). **C** shows MRI images of animals bearing SKOV3 tumors, demonstrating substantial absence of tumors and lack of ascites production in animals treated with the anti-S1P mAb. SKOV3 tumor weights were reduced 68% (**D**). For **A** and **C** n = 5 and 5, for **B** n = 10 and 15, and for **F** n = 8 and 9 mice treated with control (saline vehicle or nonspecific mAb, as indicated) and anti-S1P mAb, respectively. CD31 and H&E staining of ECs in the SKOV3 tumors (**E**) show that the anti-S1P mAb reduced tumor-associated angiogenesis and increased fibrosis. H&E staining of A549 tumors (**G**) also demonstrates that the anti-S1P mAb increased central necrosis (asterisk). In A549 tumors, isolectin staining of developed microcapillaries (**G**) and CD31 staining of ECs (**H**) both show that the anti-S1P mAb reduced tumor-associated angiogenesis (white arrows indicate tumor margins). *$p < 0.01$ for the anti-S1P mAb versus saline- or nonspecific mAb-treated mice and $^{\#}p < 0.05$ for the anti-S1P mAb versus the stop treatment. All data are represented as the mean ± SEM.

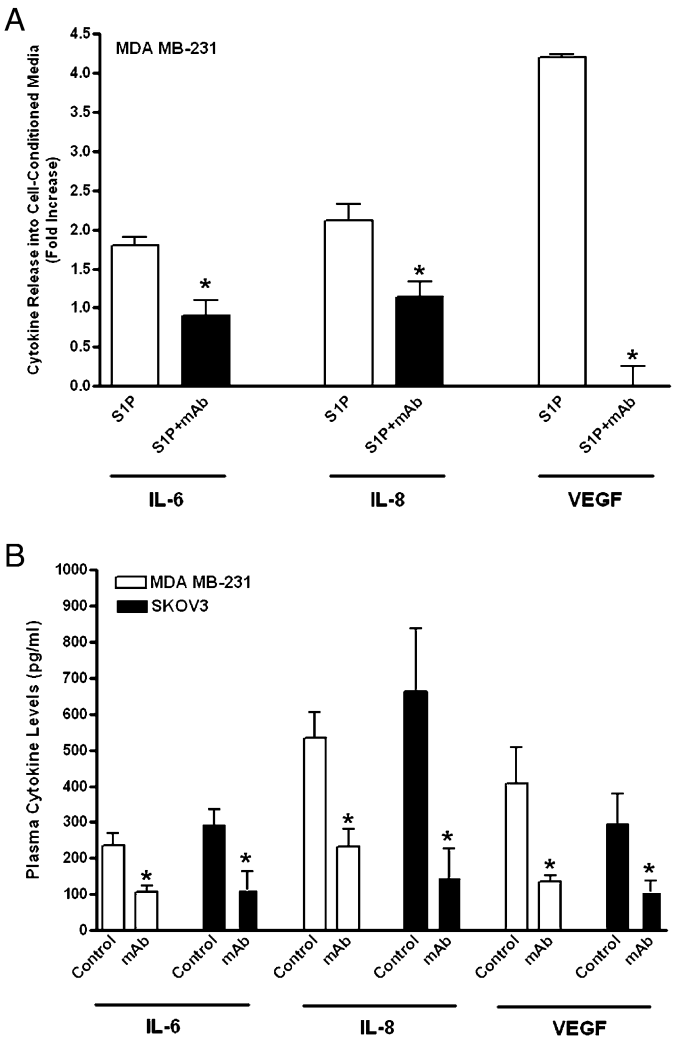

Figure 3. The anti-S1P mAb inhibits the release of proangiogenic growth factors from tumor cells in vitro and in vivo

A: Representative data demonstrating that S1P increases the release of IL-6, IL-8, and VEGF from MDA MB-231 tumor cells into the cell-conditioned media. The release is completely neutralized by incubation with 1 μg/ml of the anti-S1P mAb, in vitro.

B: Serum from MDA MB-231 and SKOV3 xenografted animals reveals the ability of the anti-S1P to reduce plasma levels of IL-6, IL-8, and VEGF. *$p < 0.05$ for the anti-S1P mAb versus saline- or nonspecific mAb-treated mice. All data are represented as the mean ± SEM.

VEGF or bFGF were mitigated by systemic treatment with the anti-S1P mAb. Quantification of data from all mice in the study (Figure 4C) shows that the VEGF- or bFGF-containing plugs from mice treated with 25 mg/kg of the anti-S1P mAb exhibited substantial reductions (82% and 89%, respectively) in blood vessel formation compared to VEGF- or bFGF-containing plugs from mice that did not receive the anti-S1P mAb. In the bFGF-containing plugs, the reduction in vascularization were dose dependent, as 1 mg/kg or 25 mg/kg of anti-S1P mAb reduced the bFGF-dependent vascularization by 32% and 89%, respectively. The ability of the anti-S1P mAb to block these effects suggests that endogenous S1P present in plasma and tissues or produced in the Matrigel plug has the ability to enhance microvascularization induced by other key proangiogenic growth factors.

The anti-S1P mAb inhibits tumor vascularization by directly influencing ECs in vitro and in vivo

Enhanced EC survival is a critical component of angiogenesis. The ability of ECs to survive depends upon circumventing cell death induced by hypoxia as well as chemotherapy. Accordingly, the ability of S1P to protect human umbilical vein endothelial cells (HUVECs) from apoptosis induced by two clinically relevant chemotherapeutic agents, doxorubicin and paclitaxel, was investigated. Figure 5A shows that HUVECs were sensitive to doxorubicin (4.4-fold increase in caspase activity after 24 hr of treatment) and, to a lesser extent, paclitaxel (2.2-fold increase). S1P induced a statistically significant reduction of caspase-3 activation in HUVECs exposed to both of the chemotherapeutic drugs (31% and 33%, respectively, for doxorubicin and paclitaxel). As expected, the addition of the anti-S1P mAb completely abolished the protective, antiapoptotic effects of S1P. Thus, S1P has the ability to protect HUVECs from the toxicity of chemotherapy agents.

The ability of ECs to migrate to the site of a tumor is also an important part of tumor-associated angiogenesis. Figure 5B shows a substantial HUVEC migration response following exposure to S1P. The addition of 1 μg/ml anti-S1P mAb to the media blocked S1P-induced migration of HUVECs by 70%.

In vitro studies have shown that S1P not only stimulates HUVEC chemotactic motility but also induces HUVEC differentiation into multicellular structures suggestive of early blood vessel formation even in the absence of growth factors (Lee et al., 1999). Figure 5C shows that serum-deprived HUVECs placed on growth factor-reduced (GFR) Matrigel failed to form capillary-like structures in the absence of S1P. Upon the addition of 1 μM S1P, HUVECs formed elongated tube-like structures after only 6 hr. The addition of the anti-S1P mAb substantially blocked the formation of the typical capillary-like structures for the duration of the experiment.

A critical stem in tumor vascularization is the infiltration and proliferation of ECs into the tumor as a consequence of the tumor-associated release of angiogenic factors. Accordingly, the ability of S1P to promote the infiltration of ECs into plugs was evaluated in vivo using the Matrigel plug assay (Figure 5D). Animals that were injected with Matrigel containing 5 μM S1P showed a substantial (>6-fold) and significant (*$p < 0.001$) increase in the density of ECs compared to those injected with Matrigel lacking S1P. The administration of anti-S1P mAb completely neutralized the ability of S1P-saturated plugs to promote cell infiltration, as no significant differences were found between antibody-treated animals and controls not treated with S1P.

Considering that the anti-S1P mAb may neutralize S1P's ability to induce the release of proangiogenic growth factors (Figure 3) and to promote de novo blood vessel formation in vivo (see Figures 2E, 2G, and 2H), one may speculate that tumor growth may depend on S1P-mediated angiogenesis, which could account for the ability of the anti-S1P mAb to retard tumor growth (Figures 2A–2D and 2F). The ability of the anti-S1P mAb to block angiogenesis was evaluated in the murine melanoma (B16-F10) allograft model. B16-F10 cells are known to be unresponsive to S1P in terms of proliferation, protection from doxorubicin-induced apoptosis, and promotion of cell migration (see below) (Arikawa et al., 2003; Yamaguchi et al., 2003). Therefore, if one were to observe an effect of the anti-S1P mAb on B16-F10 tumor growth in vivo, one could argue that this would be due to an antiangiogenic effect from the antibody rather than a direct

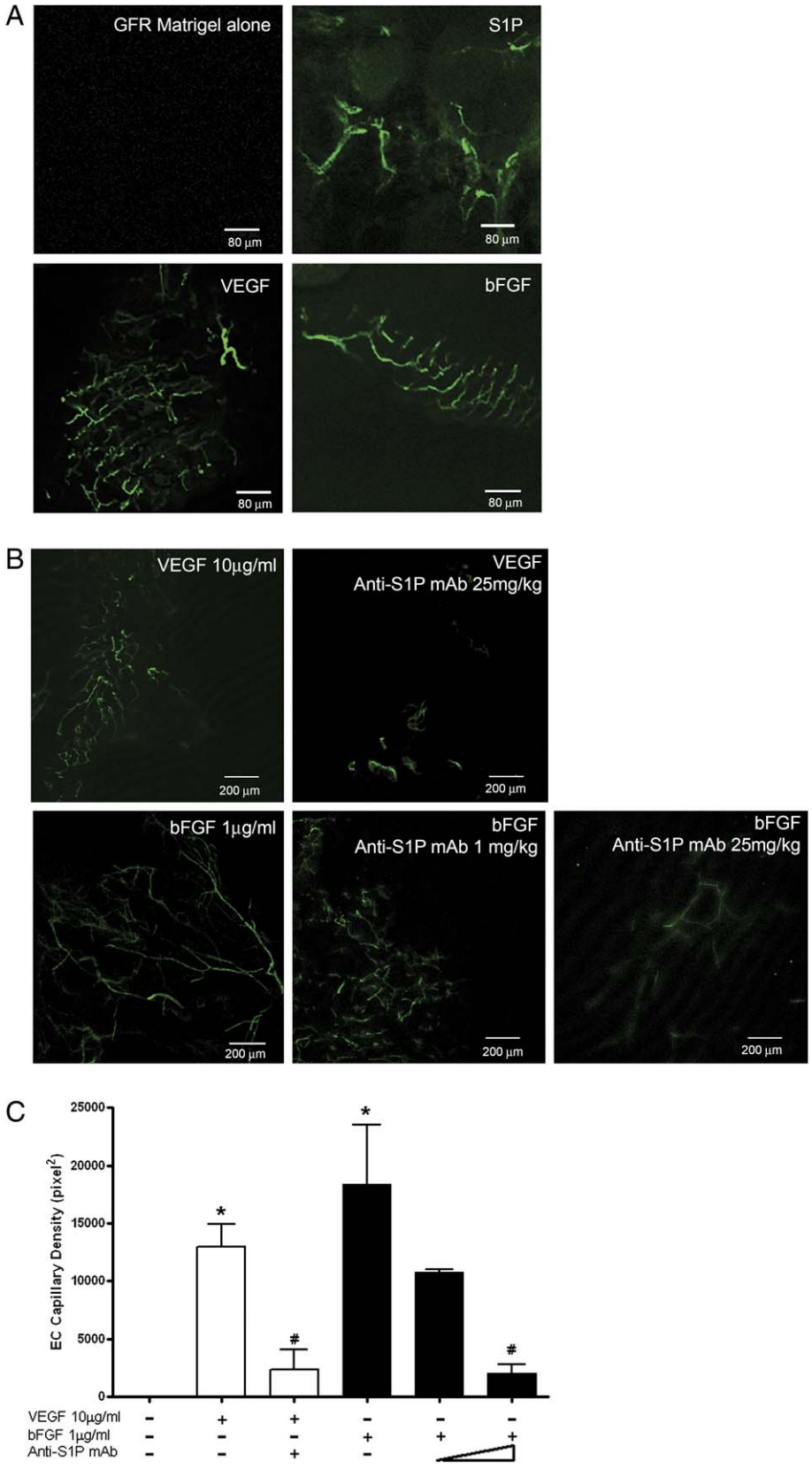

Figure 4. The anti-S1P mAb inhibits the proangiogenic effects of bFGF and VEGF in vivo

GFR Matrigel containing bFGF, VEGF, S1P, or saline was implanted into mice. Selected animals received 1 or 25 mg/kg of the anti-S1P mAb or saline every 48 hr, starting a day prior to matrix implantation. After 10 days, the plugs were harvested and analyzed for microvascular density by FITC-isolectin staining functional vessels. In **A** are representative images (scale 80 μm) showing the neovascularization effects of S1P (5 μM) compared to optimum concentrations of VEGF (10 μg/ml) and bFGF (500 ng/ml) all mixed with the GFR Matrigel prior to implantation. **B** shows representative images (scale 200 μm) of plugs premixed with either VEGF (10 μg/ml) or bFGF (1 μg/ml) prior to implantation in mice that were treated systemically with the anti-S1P mAb. **C** is a quantification of data from all treatment groups (n = 3–4 per group). Animals bearing VEGF and bFGF plugs and in treatment with 25 mg/kg of the anti-S1P mAb showed 82% and 89% reduction in tumor vasculature compared to control groups. $p < 0.001$ for *VEGF or bFGF versus saline (Matrigel alone) and $^{\#}$VEGF or bFGF versus VEGF or bFGF plus anti-S1P mAb. All data are represented as the mean ± SEM.

effect of the antibody on tumor cells. Accordingly, animals were implanted with B16-F10 melanoma cells and treated with the anti-S1P mAb. Figure 5E shows that animals treated with anti-S1P mAb exhibited on average a 57% reduction in tumor volume (and a 53% reduction in tumor weight) compared to control animals treated with saline or the nonspecific antibody. To

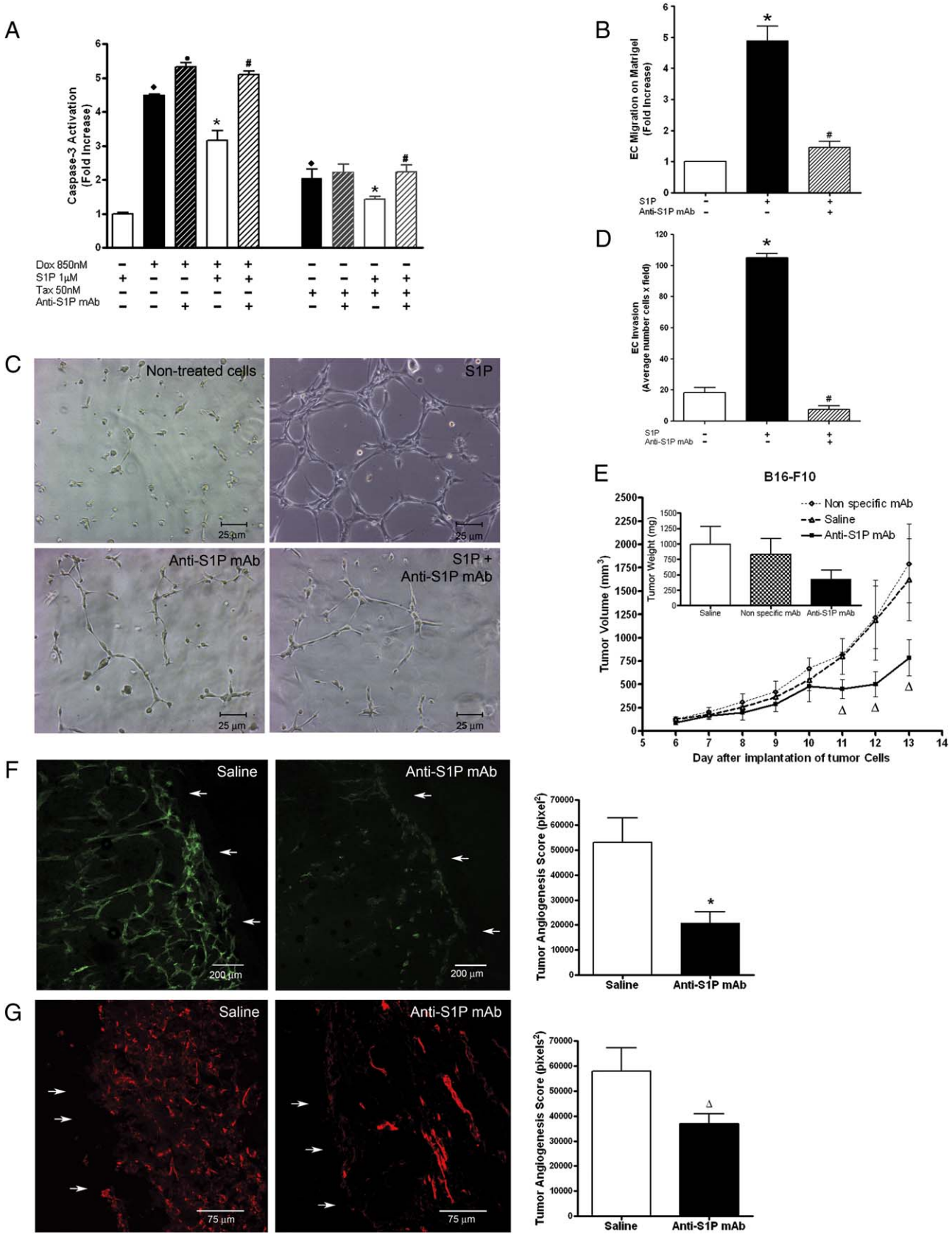

Figure 5. The anti-S1P mAb inhibits vascularization in vitro and in vivo

The anti-S1P mAb (1 μg/ml) reduced HUVEC survival against standard chemotherapeutics, doxorubicin (850 nM; Dox) or Taxol (50 nM; Tax) (**A**), migration (**B**), and the formation of capillary-like structures (**C**) when exposed to 1 μM S1P. Data are expressed as fold increases of caspase-3 activation or migrating cells

assess tumor angiogenesis after treatment with the anti-S1P mAb, we examined excised B16-F10 tumors for isolectin and CD31 staining. As Figure 5F demonstrates, treatment with the anti-S1P mAb resulted in a substantial (61%) and significant (*$p = 0.023$) reduction in tumor microcapillary density after staining with the isolectin. Similarly, Figure 5G shows that the anti-S1P mAb significantly ($^{\triangle}p < 0.05$) reduces the presence of EC density as quantified by anti-CD31 staining.

Anti-S1P mAb's direct effects on tumor cells

A variety of human tumor cell lines as well as the mouse-derived B16-F10 cells were tested in vitro for the ability of S1P to stimulate invasion, proliferation, and protection from cytotoxic agents. The in vitro Matrigel cell invasion assay was employed to evaluate cellular invasion as an indicator of metastatic potential for several cell lines (A549, HT-29, MCF-7, and B16-F10). As shown in Figure 6A, treatment with S1P induced a substantial (6- to 7-fold) increase in invasion through the Matrigel matrix in multiple tumor cell lines when compared to nontreated control cells. Only the B16-F10 cells were not stimulated by S1P in this assay. Addition of anti-S1P mAb reduced the chemotactic migration of S1P-responsive cells into the Matrigel matrix to control levels regardless of the concentration of S1P used. The dose dependence of S1P-induced invasion in the Matrigel matrix was evaluated for the A549 cell line where 1 μg/ml anti-S1P mAb neutralized all of the S1P concentrations tested (Figure S4). These results suggest that this concentration of antibody was sufficient to absorb up to 1 μM S1P as a result of the higher affinity of the antibody for S1P compared to S1P receptors on the A549 cell surfaces.

The ability of the anti-S1P mAb to neutralize S1P-induced stimulation of cellular proliferation in multiple cell lines was also evaluated. Figure 6B demonstrates the ability of S1P to increase [^{3}H]-thymidine incorporation in cells treated with 100 nM S1P when compared to nontreated control cells. The increase in DNA synthesis produced by S1P was completely mitigated by the addition of 1 μg/ml of the anti-S1P mAb.

The ability of the anti-S1P mAb to alter tumor cell survival under the stress of chemotherapeutic agents was accessed by exposing multiple tumor cell lines to 1 μM doxorubicin. Tumor cell death was assessed by the activation of the apoptotic executioner caspase-3 or H/PI (Figure 6C). As shown, S1P was able to decrease doxorubicin-induced caspase-3 activation and/or cell death to control, nontreated levels in almost all of cell types tested. With the exception of the B16-F10 cells, caspase-3 activation was increased by the anti-S1P mAb in the presence of S1P, suggesting that the protective antiapoptotic effect of S1P was eliminated by selective absorption of the lysolipid by the antibody. The ability of the anti-S1P mAb to neutralize the antiapoptotic effects of S1P depended on the dose tested

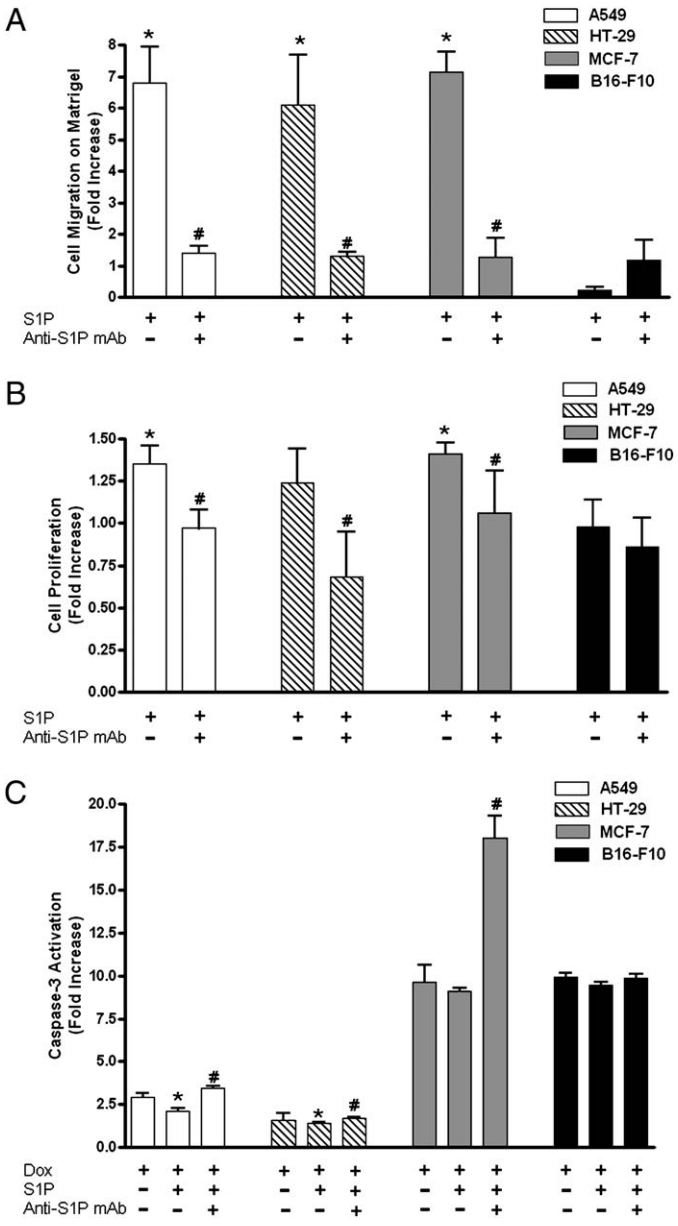

Figure 6. The anti-S1P mAb inhibits many of the protumorigenic processes

The anti-S1P mAb (1 μg/ml) mitigated S1P-induced migration (**A**), tumor cell proliferation (**B**), and cell survival against doxorubicin (Dox) (**C**) in all the tumor cell lines tested with the exception of B16-F10 cells. Data are expressed as fold increases of migrating cells, proliferation, or caspase-3 activation with respect to the control cells, in at least three independent experiments performed in triplicate. $p < 0.01$ for *S1P versus control or S1P + Dox versus Dox, and $^{\#}$S1P or S1P + Dox versus S1P + mAb or S1P + Dox + mAb. All data are represented as the mean ± SEM.

with respect to the control (taken as 1), in at least three independent experiments performed in duplicate. Matrigel plugs containing saline or 5 μM S1P were quantified for EC invasion after 10 days with Masson Trichrome (**D**). Selected animals received the anti-S1P mAb (25 mg/kg, every 48 hr). In the B16-F10 allograft model, mice bearing murine melanoma tumors were treated with saline, 25 mg/kg of the nonspecific mAb, and 25 mg/kg of the anti-S1P mAb (**E**). Data represent tumor volumes and tumor weights (inset) from nine mice per group. Animals treated with the anti-S1P mAb showed 57% and 53% reductions in tumor volumes and weights, respectively. **F** and **G** show representative images and graphic quantification of tumors stained with isolectin or CD31, respectively. White arrows indicate tumor margins. $p < 0.01$ for $^{\blacklozenge}$Dox/Tax versus saline, *S1P + Dox/Tax versus Dox/Tax, and $^{\#}$S1P + Dox/Tax versus S1P + Dox/Tax + mAb; or $p < 0.05$ for $^{\triangle}$anti-S1P mAb versus saline/nonspecific mAb and for *anti-S1P mAb versus control. All data are represented as the mean ± SEM.

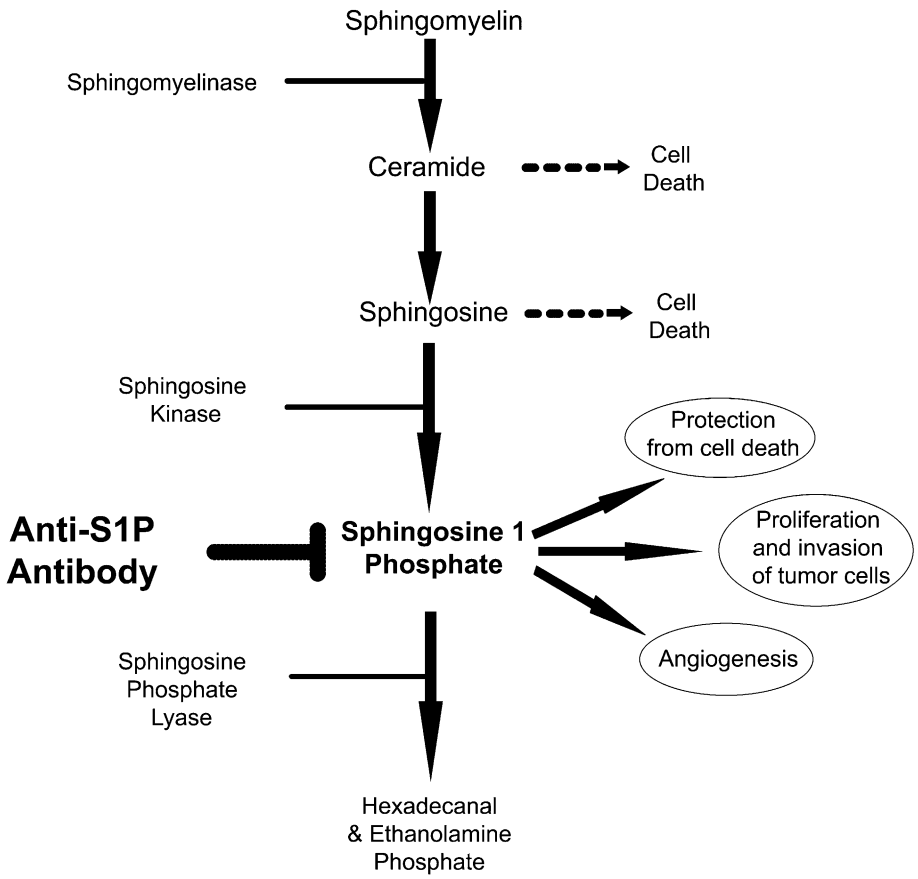

Figure 7. The sphingolipid signaling cascade

The molecular sponge concept proposed here envisions that the antibody will neutralize S1P and prevent its cancer growth-promoting effects. We also propose that the resulting decrease in the effective extracellular concentration of the protective S1P would alter the rheostat in cancer cells in favor of ceramide and sphingosine, two well-known proapoptotic signaling molecules that can be activated in cancer cells by radiation and chemotherapeutic agents. Thus, we propose that a S1P molecular sponge would have multiple mechanisms of antitumor action when used as an adjunct to standard chemotherapy or radiation therapy.

(0.001–1.0 μg/ml) (Figure S5), while the nonspecific antibody completely lacked the ability to reduce S1P-protective affects against doxorubicin-induced cell death (Figure S6).

The ability of the anti-S1P mAb to mitigate the effects of S1P in these in vitro assays suggests that (1) the mAb can effectively neutralize the direct protumorigenic effects of S1P on tumor cells; and (2) the affinity of the mAb for S1P was higher than that of the S1P receptors expressed by the tumor cells. In addition, the lack of responsiveness of the B16-F10 mouse melanoma cells to the direct actions of S1P supports the data in Figure 5F and demonstrates that S1P has a profound angiogenic effect on tumor progression.

Discussion

In this study, we used a highly specific monoclonal antibody against S1P as a molecular sponge to selectively absorb and neutralize this bioactive lipid mediator in in vitro and in vivo models designed to evaluate potential angiogenic and tumorigenic effects of S1P. The anti-S1P mAb blocked both S1P's prosurvival and angiogenic actions and has proved to be a useful tool in evaluating the actions of S1P. The ability of the anti-S1P mAb to significantly retard the progression, and in some cases eliminate established tumors of human and mouse origins, was consistent with the profound proangiogenic effects of S1P. Taken together, these data imply that the anti-S1P mAb warrants evaluation in human clinical trials.

The studies presented here suggest that a principal mechanism of the anti-S1P mAb in blocking tumor progression is through the neutralization of the proangiogenic effects of the blood-borne lipid mediator S1P. The proangiogenic effects of S1P were demonstrated in an in vivo allograft tumor model using the B16-F10 cells, in vivo with the Matrigel plug assay as well as in in vitro studies using HUVECs. Unexpectedly, the anti-S1P mAb also inhibited the release of proangiogenic cytokines in vitro and in vivo, while also potently blocking the function of VEGF and bFGF in vivo. The effects of anti-S1P mAb on VEGF and bFGF suggest either that S1P is permissive for the angiogenic effects of VEGF and bFGF or that S1P acts as the ultimate downstream mediator of VEGF and bFGF. A central and obligatory role for S1P on VEGF action, as suggested by our data, is in agreement with published results showing that VEGF receptors are transactivated by S1P (Igarashi et al., 2003). Regardless, these data confirm and validate the important role of S1P during vascularization and further suggest that the anti-S1P mAb may exhibit a wide spectrum of activity considering the complexity of the tumor environment.

In addition to the antiangiogenic effect of the anti-S1P mAb, the antibody inhibited tumor cell proliferation, invasion, and survival against standard chemotherapeutics. The reduction of tumor vasculature along with the neutralization of the prosurvival effects of S1P on tumor cells suggests that this antibody could be used as a clinical adjunct to conventional chemotherapy by sensitizing tumor cells to anticancer agents and possibly reducing the effective dose of cytotoxic chemotherapeutic agents.

The mechanism for the antitumorigenic effects of the anti-S1P mAb is simple neutralization of S1P by selective absorption. In addition to the endogenous plasma S1P, new sources of S1P in a tumor-bearing mouse could include S1P produced by tumor

cells themselves as a consequence of the upregulation of the SPHK oncogene (French et al., 2003; Johnson et al., 2005) or from stromal and inflammatory cells or other components attracted to the tumor. Regardless of the S1P source, the efficacy of anti-S1P mAb action demonstrates the importance of S1P in tumor aggressiveness and also validates the anti-S1P mAb as a potential therapeutic agent. Figure 7 shows how this strategy may be useful in cancer treatment and compares S1P as a cancer target to other key components of the sphingolipid signaling cascade. This molecular sponge concept is similar to the mechanism of action of Avastin, a humanized mAb directed against the proangiogenic growth factor VEGF (Ferrara, 2004). In contrast to the anti-VEGF strategy of neutralizing tumorigenic growth factors, most anticancer therapeutic antibodies are directed against tumor-selective antigens expressed on the surfaces of transformed cells. These therapeutic antibodies are often conjugated to radionuclides or other toxic payloads and deliver the materials to tumors by molecular targeting. The efficacy of this treatment depends, in part, on the accessibility of the antibodies to the tumor cells. As is the case for Avastin, the anti-S1P mAb used here may not suffer from this limitation in that the target, S1P, is circulating in the same compartment (i.e., blood) as is the antibody. Further, S1P is a small molecule (MW = 379 Da) and a lipid target that is thought to freely cross cell and compartment boundaries more easily than protein targets like VEGF. An additional potential advantage of an anti-S1P mAb is that the target is not species specific, as is the case with cancer targets of protein origin. S1P has the same chemical composition not only across species, but also across phyla, and it is not susceptible to mutation as a means of escaping the therapeutic.

An additional potential benefit of reducing the effective extracellular S1P concentration with the anti-S1P mAb may be in altering the sphingolipid signaling rheostat in favor of CER and SPH as it neutralizes S1P (Figure 7). CER and SPH are well-known proapoptotic intracellular signaling molecules that can be activated in cancer cells by radiation and chemotherapeutic agents (Gouaze et al., 2001; Kolesnick and Fuks, 2003) and can promote apoptosis in tumor cells (Kurinna et al., 2004), in contrast to S1P, which largely serves a protective function for cancer cells. Altering the rheostat in favor of CER would augment the anticipated ability of the anti-S1P mAb to serve as an adjunct to standard chemotherapy or radiation therapy.

Taken together, the selective absorption of S1P by a neutralizing antibody could represent a promising approach to cancer therapy. This approach may have advantages over other targets in the sphingolipid signaling cascade, such as targeting key enzymes of the S1P biosynthetic pathway responsible for S1P production (Figure 7). The pleiotropic effects of S1P in promoting tumor growth, metastasis, and angiogenesis make S1P a robust target for anticancer therapy because S1P has several mechanisms of action. Thus, the anti-S1P mAb could sensitize cancer cells to anticancer agents while exerting antiproliferative, antiangiogenic, and antimetastatic effects. The molecular sponge approach for neutralizing S1P, coupled to the finding that antibodies have favorable pharmacokinetic features and high therapeutic indices, suggest that an anti-S1P antibody may provide therapeutic benefits in treating a broad range of cancers. However, clinical trials with a humanized version of the mouse antibody will be needed to confirm this contention.

Experimental procedures

Materials

S1P, LPA, SPH, and other lipids were obtained from Avanti Polar Lipids or from Calbiochem. S1P, LPA, and SPH were complexed with fatty acid-free BSA (1 mg/ml in PBS) as a solvent-free carrier. Dulbecco's modified Eagle's medium (DMEM) and fetal bovine serum (FBS) were purchased from Invitrogen. EMB-2 medium and Bullet Kit were purchased from Cambrex. GFR and Matrigel basement membrane matrix were purchased from BD BioSciences. Anti-mouse CD31 primary antibody was obtained from Chemicon. Horseradish peroxidase (HRP)-conjugated goat anti-mouse secondary antibody and the rhodamine red-X-conjugated rabbit anti-mouse CD31 was purchased from Jackson Immunoresearch. [^{3}H]-thymidine was from Amersham Bioscience. Recombinant murine VEGF was obtained from PeproTech. Fluorescein Griffonia (Bandeiraea) Simplicifolia Lectin I, Isolectin B-4 was obtained from Vector Laboratories. High-sensitivity ELISA-based kits for cytokine determinations were purchased from R&D Systems. All other reagents were purchased from Sigma. An IgG_1 isotype-matched mouse mAb directed against a plant antigen was obtained from Strategic BioSolutions and used as a control antibody.

Cell culture

Human lung carcinoma (A549), human breast adenocarcinoma (MCF-7), human colorectal adenocarcinoma (HT-29), and the mouse melanoma (B16-F10) cell lines were obtained from American Type Culture Collections. SKOV3, MDA MB-231, and MDA MB-468 cells were obtained from the M.D. Anderson Cancer Center (Houston, TX). Cells were subcultured twice a week as per care instructions and did not exceed passage 10. HUVECs were obtained from Cambrex, maintained in EGM-2 media supplemented with EGM-2 Bullet Kit, and used between passages 3 and 8. Tumor cells were maintained in DMEM supplemented with 10% FBS, unless otherwise stated, at 37°C in a humidified 5% CO_2 atmosphere.

Animals

Four- to six-week-old female C57BL/6 and athymic nude (Ncr Nu/Nu) mice were obtained from Harland. All experiments were performed in accordance with NIH guidelines for the humane use of animals. All protocols involving the use of animals were approved by the IACUC committees at M.D. Anderson Cancer Center and San Diego State University (SDSU; protocol numbers: 04-04-010S, 04-08-020S) and conformed to all regulatory standards (NIH assurance #A3728-01 and USDA Veterinary Permit #7793).

Production of the anti-S1P mAb

For immunization, S1P was conjugated to KLH. Swiss Webster mice were immunized four times over a 2 month period with 50 μg immunogen per injection. Serum samples were collected 2 weeks after the second, third, and fourth immunizations and were screened by ELISA for the presence of anti-S1P antibodies. Spleens from animals that displayed high titers of the antibody were subsequently used to generate hybridomas using standard fusion procedures. The resulting hybridomas were grown to confluency, after which cell supernatants were collected for ELISA analysis to identify positive hybridoma clones. For ascites production, SCID mice were injected i.p. with the positive clonal cells. Monoclonal antibodies were purified by Protein A and were >95% pure by HPLC. Endotoxin levels were <3 EU/mg. The antibody was prepared in 20 mM sodium phosphate with 150 mM sodium chloride (pH 7.2) and stored at −80°C.

ELISA

Ninety-six-well high binding ELISA plates (Costar) were coated overnight with S1P diluted in PBS (137 mM NaCl, 2.68 mM KCl, 10.1 mM Na_2HPO_4, 1.76 mM KH_2PO_4; pH 7.4) containing 1% BSA at 4°C. Plates were washed with PBS and blocked with PBS/BSA for 1 hr. For the primary incubation, 0.1 μg/ml anti-S1P mAb and designated amounts of S1P, LPA, phosphatidyl serine (PS), PE, CER, C1P, SPH, dihydrosphingosine (DH-SPH), sphingomyelin (SM), SPC, and dihydrosphingosine-1-phosphate (DH-S1P) were added to wells of the ELISA plates. Plates were washed and incubated with 100 μl per well of 0.1 μg/ml HRP-conjugated goat anti-mouse secondary for 1 hr at room temperature. Plates were then exposed to tetramethylbenzidine for 1–10 min. The detection reaction was stopped by the addition of an

equal volume of 1 M H_2SO_4. Optical density of the samples was determined by measurement at 450 nm using a Thermo Multiskan EX.

Pharmacokinetic experiments

Eight-week-old C57/Bl mice were dosed with 25 mg/kg of the anti-S1P mAb i.v. and bled at designated time points. A competitive ELISA using a biotin-labeled anti-S1P mAb was used to determine the concentration of antibody remaining in the mouse blood between 20 and 120 min after the bolus dose. A standard two compartment model calculation in WinNonlin was used to determine the $t_{1/2}$ of the antibody. The experiment was repeated three times with three animals per group each time.

Toxicology study

Eight- to twenty-week-old female and male C57/Bl mice were treated with 1, 3, 10, 30, or 50 mg/kg of the anti-S1P mAb or vehicle (sterile saline) for 7 consecutive days by tail vein injection. Solutions for injection were made daily. Twenty-four hours after the final treatment, the mice were sacrificed, blood was collected by venous puncture, and organs were harvested. Whole blood and serum were sent to a veterinary testing laboratory (IDEXX Laboratories) for standard CBC and biochemical panel analysis. Tissue samples were stored in 10% formalin and shipped to a board-certified pathologist (Comparative Biosciences) for evaluation.

Cell proliferation assays

Cells were seeded onto 12-well tissue culture plates (1×10^5 cells per well) in DMEM containing 10% FBS. During treatment, cells were incubated in 10% FBS DMEM, containing either 1 mg/ml BSA in PBS as a vehicle control or various concentrations of S1P. The cells were incubated with or without anti-S1P mAb (1 μg/ml). For S1P plus antibody treatments, S1P was incubated with the anti-S1P mAb (1 μg/ml) in the media for 1 hr prior to addition to the cells. After 24 hr, cells were labeled with 1 μCi/ml [^{3}H]-thymidine and incubated for an additional 6 hr at 37°C. Labeled cells were fixed with ice-cold 10% TCA for 30 min at 4°C and then washed three times with ice-cold 10% TCA to removed unincorporated [^{3}H]-thymidine. The cells were then lysed in 1 N NaOH, and the radioactivity was counted.

Chemoinvasion assay

Cells (5×10^4 cells per well) were suspended in DMEM with 0.1% FBS and added to the top chamber of a BD BioCoat TM Invasion Systems (BD Biosciences). FBS media (10%) were used as a chemoattractant in the bottom chamber. The anti-S1P mAb (0.01, 0.1, or 1 μg/ml), and various concentrations of S1P (100 nM, 500 nM, 1 μM, and 2 μM) were preincubated for 1 hr and then added to cells in the top chamber. Tumor cells were allowed to migrate for 22 hr, at 37°C.

EC migration assays were performed using modified Boyden chambers (Corning Constar) coated with Matrigel matrix (500 μg/ml). Serum-deprived HUVECs (5×10^4 cells per well) were resuspended in minimum media (2% FBS) and added to the top chambers. S1P (100 nM) with or without the anti-S1P mAb (1 μg/ml) was added to the bottom chambers, and HUVECs were allowed to migrate for 6 hr at 37°C. After treatment, migrating cells were stained with HEMA 3 stain set (Fisher Scientific) as per the manufacturer's protocol. Five fields per filter were counted at 40× (Nikon Labophot-2). Data are expressed as the fold increases of cell invasion with respect to the nontreated control cells for at least four independent experiments performed in duplicate.

Cell death assays

Cells ($2–2.5 \times 10^5$ cells per well) were seeded into 6-well plates and allowed to grow to 80% confluence prior to treatment. The cells were then treated with and without 0.5–1 μM doxorubicin (Andriamycin) hydrochloride, 50–500 nM paclitaxel (Taxol), 0.1–1 μM S1P, and 1 μg/ml of the anti-S1P mAb, in 10% FBS DMEM for 48 hr. Treated media were replaced with fresh media after 24 hr. After 48 hr, the cells were washed twice with PBS and lysed in 85 μl of caspase assay buffer (0.5 M HEPES [pH 7.4], 10% Chaps, 0.5 M EDTA). Samples were then centrifuged at 14,000 rpm in an Eppendorf Centrifuge 5417C for 5 min to discard cellular debris. Caspase-3 activity in the supernatant was measured by caspase-3 assay kit (A.G. Scientific) according to the manufacturer's protocol and was standardized by protein determination with a BCA detection kit (Pierce). Caspase-3 activity is expressed as the fold increase in fluorescence signal with respect to nontreated cells. For the MCF-7 cells that do not express caspase-3, Hoechst/propidium iodide staining was used to evaluate cell death. At least three independent experiments were performed with triplicate runs of each condition.

EC tube-like formation assay

The formation of vascular-like structures was assessed on GFR Matrigel matrix. Tissue culture plates were coated with 300 μl of GFR Matrigel diluted 1:2 with serum-free media (0% FBS, 1 mg/ml of BSA). Matrigel was allowed to polymerize for 2 hr at 37°C. Serum-deprived HUVECs (5×10^5 cells per well) were suspended in serum-free media, seeded onto the polymerized matrix, treated with 1 μM of S1P with or without the anti-S1P mAb (1 μg/ml), and incubated at 37°C for 6 hr. Tubular networks were visualized after 6 hr at 10× (Olympus IX-70) and visualized using PhotoShop 6.0.

Cytokine release assay

Cells were starved of serum and treated with the indicated concentrations of S1P and/or the anti-S1P mAb for 22 hr. Cell-conditioned media were collected and assessed for IL-6, IL-8, and VEGF by ELISA as suggested by the manufacturer (R&D Systems). Data are presented as the fold increase with respect to nontreated cells.

In vivo matrigel plug assay

Angiogenesis in vivo was performed using the Matrigel plug assay (Staton et al., 2004). Anesthetized C56BL/6 mice were injected in the left flank with 500 μl of ice-cold GFR Matrigel. The GFR Matrigel was injected either alone (nontreated group) or with 0.5–1 μg/ml bFGF, 10 μg/ml VEGF, or 5 μM S1P. Each treatment group consisted of a minimum of three mice. Subsets of animals were treated with the anti-S1P mAb (either 1 or 25 mg/kg). Dosing of the anti-S1P mAb was initiated 1 day prior to the implantation of Matrigel, and each dose was administrated i.p. every 48 hr for the duration of the experiments. After 10 days, the mice were heparinized (12.8 mg/ml) and then injected i.v. with 200 μl of Fluorescein Griffonia (Bandeiraea) Simplicifolia I, Isolectin B-4 (0.5 mg/ml) 15 min prior to sacrifice. The plugs were excised, immediately embedded in OCT, frozen in isopentane/dry ice, sectioned (80 μm), and then mounted with coverslips using antifade mounting medium (VectaShield, Vector). Microvascular density was visualized using a Leica TCS SP2 inverted confocal microscope. Digital images were acquired using Leica Analysis Software, and the fluorescence was then quantified by PhotoShop 6.0 program and expressed as capillary density (pixel^2) by ImageJ. Selected sections (10 μm) from each treatment were also analyzed by Masson Trichrome staining. ECs infiltrating (and/or proliferating) into the plugs were counted at 100× resolution in five fields from nine sections per plug.

Xenograft and allograft mouse models

Nude mice were implanted s.c. with 2.5×10^6 A549 cells on the left flank, orthotopically into the mammary fat pads with 1×10^7 MDA MB-231 or MDA MB-468 cells or i.p. with 1×10^7 SKOV3 cells. Alternatively, 5×10^5 B16-F10 cells were implanted s.c. into the flanks of C57/Bl6 mice. Tumors were allowed to establish (75–200 or 700–800 mm^3), and then the mice were randomly divided into treatment groups (5 to 20 mice per group). Treatment groups were as follows: vehicle (saline) control, 20 mg/kg isotype-matched nonspecific mAb, 10–20 mg/kg anti-S1P mAb, and 10 mg/kg Taxol diluted to 2 mg/ml with saline. Taxol was administered once per week while all other treatments (antibodies or saline) were administered every 3 days. Measurements of tumor volume were made using calipers every 3 days by two blinded individuals and averaged. The study was terminated when the first mouse reached a maximum average volume as per IACUC standards. At the end of the study, final volumes were taken, and tumors were collected for histology. Histological features and microcapillary density were assessed by H&E, FITC-isolectinB4, and CD31 staining of vessels, respectively. For the FICT-isolectinB4 staining in the B16-F10 model, tumors from saline- and anti-S1P mAb-treated animals were sectioned (80 μm), and four sections from different regions of each tumor were selected and assessed by isolectin staining by confocal microscopy (10×). For the CD31 staining in the B16-F10, SKOV3, and A549 models, tumor sections (10 μm) were blocked overnight and stained with rat anti-mouse CD31 (1:50 dilution) and then with rhodamine red-X-conjugated rabbit anti-rat antibody (1:500 dilution), for 1 hr at room temperature each. Selected sections of each tumor were assessed by the rhodamine-X staining (40×). Each section was expressed as sum of capillary density (pixel^2) in six random fields (two in the tumor center and four in the

periphery), and values of the sections derived from each tumor were averaged. Final tumor vasculature score was expressed as the average of capillary vessel density present in the two treatment groups (n = 3/4 animals per group). Studies were completely blinded to all those collecting and analyzing the data until all data were finalized.

Magnetic resonance imaging

Animals anesthetized with inhaled isoflurane were imaged with a 4.7 T small animal MR (Bruker) axially (TE 60 ms, TR 5700 ms, 4 Nex, field of view 3.5 cm, slice thickness 1 mm with 0.3 mm skip, matrix 256 × 256, in plane resolution 150 μm) and sagittally (TE 80 ms, TR 4500 ms, 4 Nex, field of view 3.5 cm, slice thickness 1 mm with 0.3 mm skip, matrix 256 × 256, in plane resolution 230 μm) using a T2-weighted fast spin echo (FSE) sequence.

Statistical analysis

Data are presented as means ± SEM except for those shown in Figure 1C. Statistical significance of the differences between experimental groups was calculated by one-way ANOVA and an unpaired Student's t test using Graphpad software.

Supplemental data

The Supplemental Data include six supplemental figures and can be found with this article online at http://www.cancercell.org/cgi/content/full/9/3/225/DC1/.

Acknowledgments

This work was supported by NIH R43 CA110298-01 (A.L.C, R.A.S.); PO1 CA64602 and DAMD 17-02-1-0694 (G.B.M.); an International Research Doctorate on Molecular and Cellular Pharmacology (B.V.); and Lpath, Inc. R.A.S., A.L.C., W.A.G., B.J.S, B.V., K.M.M., J.A.V., and G.B.M. have stock options in Lpath, Inc.

Received: August 16, 2005
Revised: December 30, 2005
Accepted: February 23, 2006
Published: March 13, 2006

References

Allende, M.L., and Proia, R.L. (2002). Sphingosine-1-phosphate receptors and the development of the vascular system. Biochim. Biophys. Acta *1582*, 222–227.

Argraves, K.M., Wilkerson, B.A., Argraves, W.S., Fleming, P.A., Obeid, L.M., and Drake, C.J. (2004). Sphingosine-1-phosphate signaling promotes critical migratory events in vasculogenesis. J. Biol. Chem. *279*, 50580–50590.

Arikawa, K., Takuwa, N., Yamaguchi, H., Sugimoto, N., Kitayama, J., Nagawa, H., Takehara, K., and Takuwa, Y. (2003). Ligand-dependent inhibition of B16 melanoma cell migration and invasion via endogenous $S1P_2$ G protein-coupled receptor. Requirement of inhibition of cellular RAC activity. J. Biol. Chem. *278*, 32841–32851.

Beil, M., Micoulet, A., von Wichert, G., Paschke, S., Walther, P., Omary, M.B., Van Veldhoven, P.P., Gern, U., Wolff-Hieber, E., Eggermann, J., et al. (2003). Sphingosylphosphorylcholine regulates keratin network architecture and visco-elastic properties of human cancer cells. Nat. Cell Biol. *5*, 803–811.

Bektas, M., Jolly, P.S., Muller, C., Eberle, J., Spiegel, S., and Geilen, C.C. (2005). Sphingosine kinase activity counteracts ceramide-mediated cell death in human melanoma cells: role of Bcl-2 expression. Oncogene *24*, 178–187.

Clair, T., Aoki, J., Koh, E., Bandle, R.W., Nam, S.W., Ptaszynska, M.M., Mills, G.B., Schiffmann, E., Liotta, L.A., and Stracke, M.L. (2003). Autotaxin hydrolyzes sphingosylphosphorylcholine to produce the regulator of migration, sphingosine-1-phosphate. Cancer Res. *63*, 5446–5453.

Ferrara, N. (2004). Vascular endothelial growth factor as a target for anticancer therapy. Oncologist Suppl. *9*, 2–10.

French, K.J., Schrecengost, R.S., Lee, B.D., Zhuang, Y., Smith, S.N., Eberly, J.L., Yun, J.K., and Smith, C.D. (2003). Discovery and evaluation of inhibitors of human sphingosine kinase. Cancer Res. *63*, 5962–5969.

Gossmann, A., Helbich, T.H., Mesiano, S., Shames, D.M., Wendland, M.F., Roberts, T.P., Ferrara, N., Jaffe, R.B., and Brasch, R.C. (2000). Magnetic resonance imaging in an experimental model of human ovarian cancer demonstrating altered microvascular permeability after inhibition of vascular endothelial growth factor. Am. J. Obstet. Gynecol. *183*, 956–963.

Gouaze, V., Mirault, M.E., Carpentier, S., Salvayre, R., Levade, T., and Andrieu-Abadie, N. (2001). Glutathione peroxidase-1 overexpression prevents ceramide production and partially inhibits apoptosis in doxorubicin-treated human breast carcinoma cells. Mol. Pharmacol. *60*, 488–496.

Igarashi, J., Erwin, P.A., Dantas, A.P., Chen, H., and Michel, T. (2003). VEGF induces $S1P_1$ receptors in endothelial cells: implications for cross-talk between sphingolipid and growth factor receptors. Proc. Natl. Acad. Sci. USA *100*, 10664–10669.

Ignoffo, R. (2004). Overview of bevacizumab: a new cancer therapeutic strategy targeting vascular endothelial growth factor. Am. J. Health Syst. Pharm. *61*, S21–S26.

Johnson, K.R., Johnson, K.Y., Crellin, H.G., Ogretmen, B., Boylan, A.M., Harley, R.A., and Obeid, L.M. (2005). Immunohistochemical distribution of sphingosine kinase 1 in normal and tumor lung tissue. J. Histochem. Cytochem. *59*, 1159–1166.

Kolesnick, R., and Fuks, Z. (2003). Radiation and ceramide-induced apoptosis. Oncogene *22*, 5897–5906.

Kurinna, S.M., Tsao, C.C., Nica, A.F., Jiffar, T., and Ruvolo, P.P. (2004). Ceramide promotes apoptosis in lung cancer-derived A549 cells by a mechanism involving c-Jun NH2-terminal kinase. Cancer Res. *64*, 7852–7856.

Kwon, Y.G., Min, J.K., Kim, K.M., Lee, D.J., Billiar, T.R., and Kim, Y.M. (2001). Sphingosine 1-phosphate protects human umbilical vein endothelial cells from serum-deprived apoptosis by nitric oxide production. J. Biol. Chem. *276*, 10627–10633.

Lee, O.H., Kim, Y.M., Lee, Y.M., Moon, E.J., Lee, D.J., Kim, J.H., Kim, K.W., and Kwon, Y.G. (1999). Sphingosine 1-phosphate induces angiogenesis: its angiogenic action and signaling mechanism in human umbilical endothelial cells. Biochem. Biophys. Res. Commun. *264*, 743–750.

Licht, T., Tsirulnikov, L., Reuveni, H., Yarnitzky, T., and Ben-Sasson, S.A. (2003). Induction of pro-angiogenic signaling by a synthetic peptide derived from the second intracellular loop of S1P3 (EDG3). Blood *102*, 2099–2107.

Maceyka, M., Payne, S.G., Milstien, S., and Spiegel, S. (2002). Sphingosine kinase, sphingosine-1-phosphate, and apoptosis. Biochim. Biophys. Acta *1585*, 193–201.

Ogretmen, B., and Hannun, Y.A. (2004). Biologically active sphingolipids in cancer pathogenesis and treatment. Nat. Rev. Cancer *4*, 604–616.

Radeff-Huang, J., Seasholtz, T.M., Matteo, R.G., and Brown, J.H. (2004). G protein mediated signaling pathways in lysophospholipid induced cell proliferation and survival. J. Cell. Biochem. *92*, 949–966.

Richieri, G.V., Anel, A., and Kleinfeld, A.M. (1993). Interactions of long-chain fatty acids and albumin: determination of free fatty acid levels using the fluorescent probe ADIFAB. Biochemistry *32*, 7574–7580.

Schwartz, B.M., Hong, G., Morrison, B.H., Wu, W., Baudhuin, L.M., Xiao, Y.J., Mok, S.C., and Xu, Y. (2001). Lysophospholipids increase interleukin-8 expression in ovarian cancer cells. Gynecol. Oncol. *81*, 291–300.

Spiegel, S., and Milstien, S. (2003). Sphingosine-1-phosphate: an enigmatic signalling lipid. Nat. Rev. Mol. Cell Biol. *4*, 397–407.

Staton, C.A., Stribbling, S.M., Tazzyman, S., Hughes, R., Brown, N.J., and Lewis, C.E. (2004). Current methods for assaying angiogenesis in vitro and in vivo. Int. J. Exp. Pathol. *85*, 233–248.

Takuwa, Y. (2002). Subtype-specific differential regulation of Rho family G proteins and cell migration by the Edg family sphingosine-1-phosphate receptors. Biochim. Biophys. Acta *1582*, 112–120.

Van Brocklyn, J.R., Jackson, C.A., Pearl, D.K., Kotur, M.S., Snyder, P.J., and Prior, T.W. (2005). Sphingosine kinase-1 expression correlates with poor survival of patients with glioblastoma multiforme: roles of sphingosine kinase isoforms in growth of glioblastoma cell lines. J. Neuropathol. Exp. Neurol. *64*, 695–705.

Wang, F., Van Brocklyn, J.R., Hobson, J.P., Movafagh, S., Zukowska-Grojec, Z., Milstien, S., and Spiegel, S. (1999). Sphingosine 1-phosphate stimulates cell migration through a G(i)-coupled cell surface receptor. Potential involvement in angiogenesis. J. Biol. Chem. *274*, 35343–35350.

Xia, P., Gamble, J.R., Wang, L., Pitson, S.M., Moretti, P.A., Wattenberg, B.W., D'Andrea, R.J., and Vadas, M.A. (2000). An oncogenic role of sphingosine kinase. Curr. Biol. *10*, 1527–1530.

Yamaguchi, H., Kitayama, J., Takuwa, N., Arikawa, K., Inoki, I., Takehara, K., Nagawa, H., and Takuwa, Y. (2003). Sphingosine-1-phosphate receptor subtype-specific positive and negative regulation of Rac and haematogenous metastasis of melanoma cells. Biochem. J. *374*, 715–722.